Exploring the potential of antihyperons in nuclei with antiprotons

J. Pochodzalla

Johannes Gutenberg-Universität Mainz, Institut für Kernphysik, D-55099 Germany

Abstract

A simple method to explore the interaction of antihyperons in nuclei by exclusive hyperon-antihyperon pair production close to threshold in antiproton nucleus interactions is proposed. Due to energy and momentum conservation event-by-event transverse momentum correlations of the produced hyperons and antihyperons contain information on the difference between their potentials. A schematic Monte Carlo simulation is used to illustrate the sensitivities of the proposed method for the reaction 1.66 GeV/c $\overline{\mathrm{p}}^{12}\mathrm{C} \rightarrow \Lambda\overline{\Lambda}$. For produced D-meson pairs at 6.7 GeV/c the sensitivity of the transverse momenta correlation will probably be too small to deduce differences between the potentials for D^+ and D^- mesons. However, for $\Xi\overline{\Xi}$ pairs produced at 2.9 GeV/c the asymmetry is sufficiently sensitive to predicted differences between the Ξ and $\overline{\Xi}$ potentials.

Key words:
PACS: 25.70.Pq, 21.80.+a

Based on G-parity transformation [1] Dürr and Teller predicted within an early form of a relativistic field theory a strongly attractive potential for antiprotons in nuclei [2, 3]. It is however obvious that G-parity transformation can provide a link between the NN and $N\overline{N}$ interaction at most for distances where meson exchange is a valid concept [4, 5]. For distances lower than about 1 fm, quark degrees of freedom may play a decisive role. The study of the potential of antibaryons in nuclei may therefore help to elucidate the role of the quark-gluon structure of baryons for the short-range baryon-baryon force.

Early studies of antiproton-nucleus scattering cross sections [6, 7] showed however disagreement with such a strong attractive potential. Later, X-ray transitions in antiprotonic atoms [8, 9, 10, 11] (an overview on subsequent experimental studies can be found in Ref. [12]) gave also hints for an attractive potential albeit with large uncertainties [13, 14]. Other analyses favor shallow real and deep imaginary potentials (for example [15]). More comprehensive studies [16] of antiprotonic X-rays as well as recent analyses of the production of antiprotons in reactions with heavy ions resulted in real attractive potentials in the range of about -100 to -150 MeV [17, 18, 19].

Concerning baryons beyond SU(2), only for Λ hyperons reliable information on their nuclear potential is available from hypernuclei studies. No experimental information on the nuclear potential of antihyperons exists so far. Mishustin and co-workers recently suggested to study deeply bound antibaryonic nuclei via various characteristic signals in their decay process [20, 21], like the production of multi-quark-antiquark clusters, multifragmentation events with strong radial flow or sharp lines in meson spectra due to transitions from the Fermi to the Dirac sea. From the experimental point of view it is however not obvious whether these proposed observables will provide unique and quantitative signals of deeply bound antibaryonic systems.

In this letter we show that quantitative information on the antihyperon potentials relative to that of the corresponding hyperon may be obtained via exclusive antihyperon-hyperon pairs production close to threshold after an antiproton-proton annihilation within a complex nucleus (Fig. 1). Once these hyperons leave the nucleus and are detected, their asymptotic momentum distributions will reflect the depth of the respective potentials. A deep potential for one species could result in a momentum distribution of antihyperons which differs from that of the coincident hyperon. This situation is in line with the case of antiprotons produced in heavy ion collisions close to threshold [17, 18, 19]. The advantage here is, that we are dealing with a quasi stationary system having a reasonably well defined geometry and that the kinematics is determined essentially by energy and momentum conservation of a (nearly) two-body reaction. However, since in the $\overline{\mathrm{p}}\mathrm{p}$ center-of-mass the distribution of the produced baryon-antibaryon pair will usually not be isotropic, the analysis can rely only on the *transverse* momenta of the outgoing baryons: because the initial average transverse momentum is equal to zero and neglecting for the moment rescattering and the Fermi motion of the struck proton (both effects will be discussed below) the magnitude of the transverse momenta of the produced baryons and antibaryons will be equal unless there is a difference in the

Email addresses: pochodza@kph.uni-mainz.de (J. Pochodzalla)

Table 1: Scalar and vector potentials, S and V, used in the model calculations. The first three columns give the default values for p $\overline{\text{p}}$ and Λ hyperons used in the parameter scans which are presented in Fig. 2 and Fig. 3. The values in the last 8 columns were adopted from Ref. [38, 39] and are used in the calculations shown in Fig. 4.

potential	p	$\overline{\text{p}}$	Λ	p	$\overline{\text{p}}$	Λ	$\overline{\Lambda}$	Ξ	$\overline{\Xi}$	D^+	D^-
V [MeV]	300	200	200	125	-125	84	-84	42	-42	-42	42
S [MeV]	-342	-342	-228	-184	-184	-123	-123	-61	-61	-61	-61
V+S [MeV]	-42	-142	-28	-59	-309	-39	-207	-19	-103	-103	-19

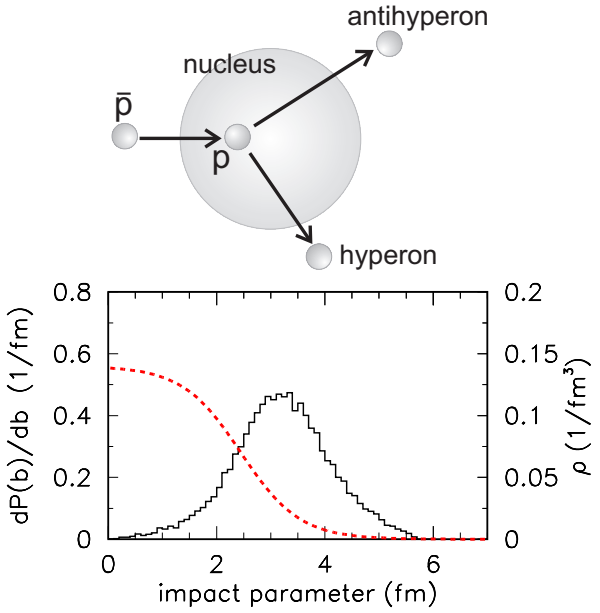

Figure 1: Scheme of the reaction proposed to explore the nuclear potentials of the baryon and the antibaryon (top). The lower part shows the probability density distribution of the impact parameter leading to the observation of a $\Lambda\overline{\Lambda}$ pair in 1.66 GeV/c $\overline{\text{p}}^{12}$C$\rightarrow$ $\Lambda\overline{\Lambda}$ reactions. In these simulations default parameters as discussed in the text have been used. For orientation the dashed line gives the assumed radial density of the ^{12}C nucleus (right scale).

effective potentials.

In the following we explore the influence of the potentials on the transverse momentum distributions of the coincident hyperons and antihyperons as well as on their event-by-event correlations by means of a schematic Monte Carlo simulation. Albeit crude, this classical approach allows to explore the role of different features of the reaction in a transparent way. As an example we consider the $\overline{\text{p}}^{12}\text{C} \rightarrow \Lambda\overline{\Lambda}$ reaction at 1.66 GeV/c, where existing data [22, 23] demonstrate the feasibility of such measurements. Since the method relies essentially on momentum and energy conservation, an extension to other hadron-antihadron pairs produced exclusively in antiproton-nucleus collisions close to their respective thresholds is straight forward. In future, such reactions can be studied at the international Facility for Antiproton and Ion Research FAIR [24] with e.g. the planned $\overline{\text{P}}$ANDA experiment [25].

The absorption of the antiprotons entering the target nucleus determines the points of annihilation inside the nucleus and the paths which the eventually produced hyperons and antihyperons have to pass inside the nucleus prior to emission. For the proton density we adopted a Fermi-type distribution

$$\rho(r) = \frac{\rho_0}{1 + exp((r - r_0 \cdot A^{1/3})/d_0)}, \quad (1)$$

where r denotes the radial distance from the center of the target nucleus and A its mass number. For the radius parameter r_0 and the surface diffuseness d_0 default values of 1.07 fm and 0.54 fm were used [26]. Since in the following we focus on light nuclei, equal neutron and proton density distributions were assumed.

The initial $\overline{\text{p}}$p annihilation is controlled by an $\overline{\text{p}}$N annihilation cross section of 50 mb [27]. The lower part of Fig. 1 shows the probability density distribution of the impact parameter leading to the emission of a $\Lambda\overline{\Lambda}$ pair in 1.66 GeV/c $\overline{\text{p}}^{12}\text{C} \rightarrow \Lambda\overline{\Lambda}$ reactions. For orientation the dashed line gives the assumed radial density profile of the ^{12}C nucleus. Because of the strong absorption of the antihyperons, the *emitted* hyperon-antihyperon pairs are - unlike in inclusive reactions [28, 29] - created close to the corona of the target nucleus at an average impact parameter of 3.1 fm and a typical density of 20 to 25% of the central nuclear density.

For both, the emitted Λ's and the $\overline{\Lambda}$'s the inverse of the average integrated path weighted with the local density along the path $\langle \int \rho ds \rangle^{-1}$ varies for the parameter range discussed in this paper in the range from about 800 to 1600 mb. For our default parameters this value is about 1000mb and thus significantly larger than the typical elastic cross sections in the relevant momentum range of <200mb. As a consequence re-scattering effects are expected to be small and have been neglected in our model. Experimentally, re-scattering effects with momentum transfers beyond the typical Fermi momentum can possibly be reduced by constraining the azimuthal angle between the hadron and antihadron momentum.

In reactions close to threshold the Fermi motion of the protons inside the nuclear target contributes significantly to the final momenta. Hence the initial proton momentum was sampled from a distribution

$$dP(p, \theta, \phi) \propto (1+e^{(E-E_F)/kT})^{-1} p^2 \sin(\theta) dp \; d\theta \; d\phi \quad (2)$$

where a default Fermi energy E_F corresponding to a momentum of p_F= 220 MeV/c was used [30]. Quasifree me-

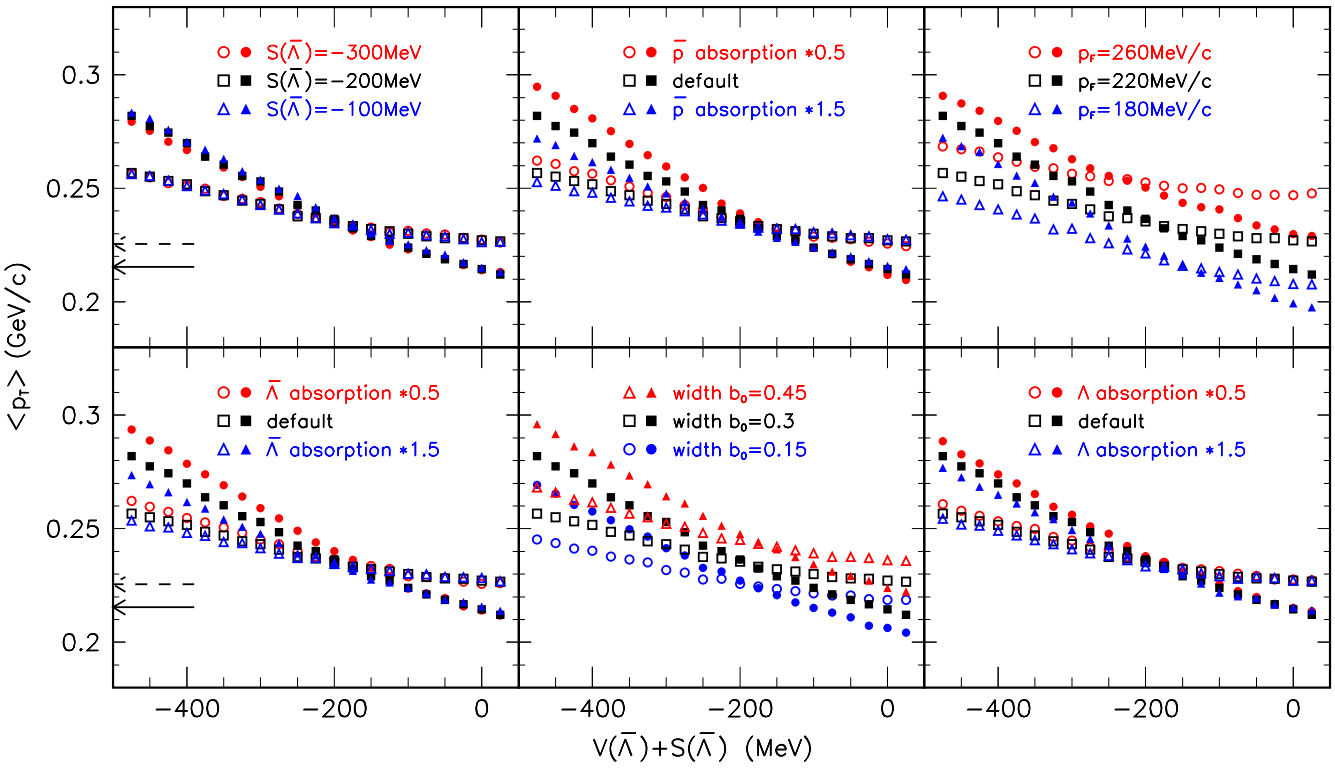

Figure 2: Transverse momentum of $\overline{\Lambda}$ hyperons (open symbols) and Λ hyperons as a function of the total $\overline{\Lambda}$ potential for different parameter sets. The dashed and solid arrows mark the result for $\overline{\Lambda}$ and Λ if all individual Λ and $\overline{\Lambda}$ potentials are set to 0.

son scattering experiments suggest [31, 32, 33] that owing to the fact that the $\overline{\mathrm{p}}$p annihilations happens in the periphery of the target nucleus at subsaturation density, significantly lower Fermi momenta may be expected. We therefore varied p_F in the range of 180 to 260 MeV/c. For the diffuseness parameter a value of T= 1 MeV was used and the maximum possible energy was determined by E_F+E_B, where E_B=8 MeV denotes the typical nucleon binding energy.

Antilambdas produced in $\overline{\mathrm{p}}$p annihilations are emitted preferentially in the direction of the incident antiproton [22]. For the 1.66 GeV/c $\overline{\mathrm{p}}^{12}$C $\rightarrow \Lambda\overline{\Lambda}$ reaction [22, 34, 35] the probability distribution of the center of mass angle θ_{cm} of the outgoing antihyperon can be described by:

$$dP(\theta_{cm}) \propto \frac{a_0 + \exp((\cos\theta_{cm} - 1)/b_0)}{1 + a_0} d(\cos\theta_{cm}) \quad (3)$$

with default values for the constant term a_0 and the width b_0 of 0.1 and 0.3, respectively.

Lacking any detailed experimental information it is plausible to assume that the annihilation cross sections for antihyperons show a similar momentum dependence as the $\overline{\mathrm{p}}$p system [36]. We therefore parameterized the absorption cross section of the $\overline{\Lambda}$ as

$$\sigma_{\overline{\Lambda}N}^{ann} = 100mb/(p_{\overline{\Lambda}} + 1) \quad (4)$$

with the $\overline{\Lambda}$ momentum given in GeV/c. For the Λ hyperons a momentum independent inelastic cross section of 20 mb was adopted.

The energy and the momentum of the baryons propagating within the nucleus are related according to [37]:

$$(E - V)^2 = (M_0 + S)^2 + \mathbf{P_{in}}^2 \quad (5)$$

Here V and S denote the real part of the vector and scalar potential, respectively. The relation between the momenta inside and outside of the nuclear potential are approximated by

$$\mathbf{P_{out}}^2 + M_0^2 = (\sqrt{(M_0 + S)^2 + \mathbf{P_{in}}^2} + V)^2. \quad (6)$$

Refractive effects at the potential boundary were ignored. For simplicity no momentum dependence of these potentials was considered in our schematic simulation. The default parameters for the scaler and vector potentials of the various baryons at normal nuclear density ρ_0 are listed in Tab. 1. For the proton and the Λ hyperon (given by 2/3 of that of the proton) these values give rise to typical total potentials of -42 and -28 MeV, respectively. For the antiproton the summed potential is in the range of the more recent experimental results [16, 17, 18, 19].

Since the antiproton annihilation and the subsequent $\overline{\Lambda}\Lambda$-pair production take place in the nuclear periphery at low densities ρ (see Fig. 1), the local potentials are expected to be reduced. We assumed for simplicity a linear density dependence $\propto \rho/\rho_0$ for all vector and scalar potentials. All numbers for potentials quoted below refer to the value at normal nuclear density ρ_0.

In a last step a finite momentum resolution of 10% was applied to mimic possible experimental uncertainties.

Fig. 2 shows the average transverse momenta of Λ hyperons (closed symbols) and $\overline{\Lambda}$ hyperons (open symbols) as a function of the total $\overline{\Lambda}$ potential $V(\overline{\Lambda}) + S(\overline{\Lambda})$ for various parameter sets. In all plots the black points result from the default parameter set. The transverse momenta of the $\overline{\Lambda}$ hyperons drop with decreasing depth of the total $\overline{\Lambda}$ potential. For the Λ hyperons this drop is even more pronounced. This surprising behavior can be traced back to the imposed momentum conservation and the different sign of the vector potentials for hyperons and antihyperons. Thus within our schematic model an agreement between the transverse momenta of hyperons and antihyperons would not necessarily imply that both encounter identical potentials.

Even if all antihyperon and hyperon potentials are set to zero one finds different average transverse momenta for $\overline{\Lambda}$'s and Λ's of 225 and 215 MeV/c, respectively. They are marked by the dashed and solid arrows in Fig. 2. This difference is caused by the anisotropy in the θ_{cm}-distribution (Eq. 3) and the relativistic transformation of the isotropic Fermi momentum. We checked that if either the assumed Fermi momentum distribution in the target is switched off or if an isotropic θ_{cm}-distribution is assumed one obtains equal average transverse momenta for Λ and $\overline{\Lambda}$ hyperons. The largest sensitivities to variations of the model parameters are observed for the assumed Fermi momentum (left middle panel) and the assumed anisotropy (left lower panel). For all other parameters the sensitivity of p_T is significantly weaker. Thus, the simultaneous measurement of transverse momenta of hyperons and antihyperons can be used to adjust the Fermi momentum in the calculations.

Studying only the average transverse momentum distributions separately does obviously not allow to extract unambiguous information on the potential of antihyperons. On the other hand, a difference between transverse momenta of the concident hadron and antihadron within one event reflects directly the different potentials. In order to study this correlation and to reduce the influence of the center of mass angle θ_{cm} we suggest to explore the transverse momentum asymmetry α_T as a function of the longitudinal asymmetry α_L. Here, α_T and α_L are defined for each event in terms of the transverse and longitudinal momenta, respectively:

$$\alpha_T = \frac{p_T(\Lambda) - p_T(\overline{\Lambda})}{p_T(\Lambda) + p_T(\overline{\Lambda})} \quad , \quad \alpha_L = \frac{p_L(\Lambda) - p_L(\overline{\Lambda})}{p_L(\Lambda) + p_L(\overline{\Lambda})}. \quad (7)$$

The Fermi motion of the struck proton inside the target may provide a total transverse momentum which will be different for each event. However, in case the scalar and vector potentials of hyperons and antihyperons are equal, the average $\langle \alpha_T \rangle$ is expected to be 0 except for small asymmetries caused by the combined effect of the Fermi motion, the anisotropic angular distribution and the different absorption cross sections for $\overline{\Lambda}$'s and Λ's.

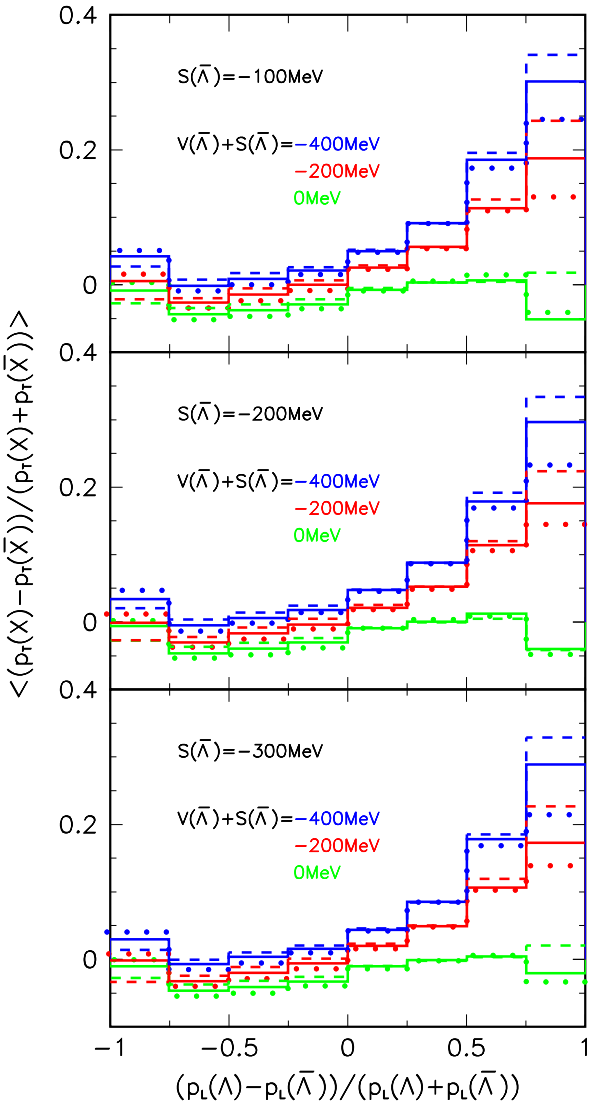

Figure 3: Average transverse momentum asymmetry as a function of the longitudinal momentum asymmetry for different parameter pairs of the scaler and vector $\overline{\Lambda}$ potentials. In each panel calculations with 3 different Fermi momenta of 180 MeV/c (dashed lines), 220 MeV/c (solid lines), and 260 MeV/c (dotted lines) are overlaid.

The histograms in fig. 3 show the average transverse asymmetry $\langle \alpha_T \rangle$ for various bins in α_L. Calculations were done for three different scalar potential $S(\overline{\Lambda})$ of -100, -200, and -300 MeV, respectively. In each panel, the different colored histograms are the results for total potentials of $V(\overline{\Lambda})+S(\overline{\Lambda})$=0, -200 and -400 MeV, respectively. Furthermore, in each plot calculations with three different Fermi momenta of 180, 220, and 260 MeV/c are overlaid. For all other parameters the default values were used. Variations in the first and last bins are partly caused by the low number of events in these bins resulting in statistical errors $\delta\alpha_T \simeq 0.01$ and 0.02, respectively. While the average transverse momenta are very sensitive to the choice of the Fermi momentum, the transverse momentum asymmetry is not. Using different parametrizations of the Fermi mo-

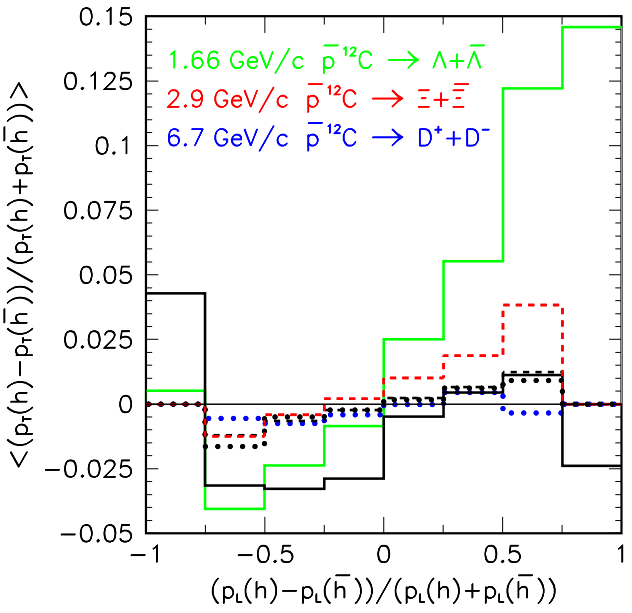

Figure 4: Average transverse momentum asymmetry of $\Lambda\overline{\Lambda}$(solid green line), $\Xi\overline{\Xi}$ (red dashed line) and D^+D^- pairs (blue dotted line) produced exclusively in 1.66, 2.9 and 6.7 GeV/c $\overline{p}^{12}$C interactions, respectively. In these calculations the potentials given in the last eight columns of Table 1 were used. The black solid, dashed and dotted histograms are the result if all scalar and vector potentials of the produced $\Lambda\overline{\Lambda}$, $\Xi\overline{\Xi}$ and D^+D^- pairs are set to 0. Asymmetries identical to 0 in the first and last bins signal zero counts.

tion (based e.g. on a local density approximation) gave rather similar final results provided the Fermi momentum parameter was tuned to similar average transverse hyperon and antihyperon momenta. Indeed, for a given Λ potential, α_T is mainly determined by the total potential $V(\overline{\Lambda})+S(\overline{\Lambda})$ as indicated by the overlap of the histograms of the same color. At negative values of α_L the $\overline{\Lambda}$ momenta are relative large and consequently the sensitivity of α_T to the potential is weaker.

The average transverse asymmetry is non-zero even if the total potential $V(\overline{\Lambda}) + S(\overline{\Lambda})$=0 (green histograms). A very similar behavior is found even if all scalar and vector potentials for $\overline{\Lambda}$ and Λ are set to 0. Like in the case of the average p_T, this is caused by the interplay between the isotropic Fermi motion and the anisotropic cm-distribution and - although less important - by the different absorption cross section. Also the assumed scaling of the momentum resolution with the absolute momentum causes a small positiv correlation between α_T and α_L. We also checked that the results are rather robust despite significant changes - by typically ±50% - of all other parameters like absorption cross sections and (anti)proton potentials. Systematic relative shifts remained usually below $\delta\alpha/\alpha = \pm 0.15$. Furthermore, neglecting the momentum dependence of the $\overline{\Lambda}$ absorption and assuming constant absorption cross sections of 100mb and 20mb yields asymmetries very similar to the momentum dependent cross section of Eq. 4 scaled by a factor 1.5 and 0.5, respectively.

As already mentioned before, this kinematic method of transverse momentum correlations can in principle be applied to each hadron-antihadron pair produced exclusively in $\overline{p}A$ interactions. As an example, the colored solid, dashed and dotted histograms in figure 4 show the average transverse momentum asymmetry of $\Lambda\overline{\Lambda}$, $\Xi\overline{\Xi}$ and D^+D^- pairs produced in 1.66, 2.9 and 6.7 GeV/c $\overline{p}$ + ^{12}C interactions, respectively. For simplicity, isotropic center-of-mass distributions were assumed in case of the $\Xi\overline{\Xi}$ and D^+D^- production. For the Ξ and $\overline{\Xi}$ baryons the same absorption cross sections as for the Λ and $\overline{\Lambda}$ were adopted, whereas for D^- and D^+ mesons energy independent absorption cross sections of 10 and 90mb, respectively, were taken. The scalar and vector potentials were inspired by Refs. [38, 39] and are listed in Tab. 1. To mimic experimental effects a relative resolution for the momentum reconstruction of 5% was also taken into account.

For orientation, the black histograms in Fig. 4 show the asymmetries if all scalar and vector potentials of the outgoing hadrons and antihadrons are set to 0. While for $\Xi\overline{\Xi}$ (dashed) and D^+D^- pairs (dotted) these histograms are symmetric around α_L=0, it is not the case for $\Lambda\overline{\Lambda}$ pairs (solid line). As already mentioned before, this is caused by the assumed anisotropic c.m.-distribution of the $\Lambda\overline{\Lambda}$ production.

Also these calculations confirm the robustness of the transverse momentum asymmetry with respect to variations of the model parameters: as expected from the similar values for S and V (Tab. 1), the asymmetries for the $\Lambda\overline{\Lambda}$ pairs (green histogram in Fig. 4) are indeed close to the red histograms shown in Fig. 3. We also would like to note that a quite similar result is found for $\Sigma^-\overline{\Sigma}^+$ pairs. In a purely classical, non-relativistic picture the asymmetry is of the order of $\Delta U/4 \cdot E_0$, where ΔU is the potential difference and E_0 the typical kinetic energy of the hadrons. In line with this consideration the large laboratory momenta of the Ξ hyperons and the D mesons explain the smaller asymmetries for the heavier particles.

To demonstrate the experimental feasibility of the proposed measurement one may consider as an example the bins of 0.25≤ α_T < 0.5 and 0.5≤ α_T < 0.75 where a sizable asymmetry is predicted. Depending on the choice of parameters these bins contain approximately 6-10% and 1-3%, respectively, of the total number of events. The α_T-distributions have a typical width of 0.3. At the expected $\Lambda\overline{\Lambda}$ detection rates at $\overline{\mathrm{P}}$ANDA [41] measurement periods of a few minutes will be sufficient to reach a relative statistical uncertainty of better than 10% for α_T within these two bins. Given the relative large cross section for $p\overline{p}\rightarrow$ $\Xi\overline{\Xi}$ at 2.9 GeV/c of ∼1μb [40] the sensitivity of the transverse asymmetry (dashed histograms in Fig. 4) is sufficiently large to explore the $\Xi\overline{\Xi}$ pair production at the future FAIR facility. In case of $\Xi\overline{\Xi}$ pairs a measurement of α_T with a precision of 10% in the same two bins will require typically 2 and 10 hours, respectively. For D-meson

pairs, however, the large momenta relative to the target remnant (> 3 GeV/c) and the low production cross section ($\sim$10nb) casts a meaningful measurement of the transverse momentum asymmetry in doubt for the case of the potential difference of $\approx$50-100 MeV given in Tab. 1. (cf. the dotted black and dotted blue histograms in Fig. 4). Only for significantly deeper potentials than the ones listed in Tab. 1 a measurable asymmetry can be expected. But even then the estimated measurement periods will significantly exceed one month.

The fact that energy and momentum conservation are the main ingredient of the proposed method raises hope that similar results might be obtained by more realistic calculations taking for example the momentum dependence of the potentials into account. Since most of the *emitted* hyperon-antihyperon pairs are created in the nuclear periphery at subsaturation density, a neutron skin of neutron rich target nuclei may help to explore different effective potentials. Significant deflections at the potential boundary which are ignored in the present work may be at least partly eliminated by demanding that the target nucleus remains intact. Furthermore, it may be interesting to study questions related to e.g. the formation time [42] by using target nuclei of different size.

The author thanks S. Pomp, T. Johansson and W. Eyrich for helpful discussions. We acknowledge financial support from the Bundesministerium für Bildung und Forschung (bmb+f) under contract number 06MZ225I.

References

[1] T.D. Lee and C.N. Yang, Nuovo Cim. **3**, 749 (1956).
[2] Hans-Peter Dürr and Edward Teller, Phys. Rev. **101**, 494 (1956).
[3] Hans-Peter Dürr, Phys. Rev. **103**, 469 (1956).
[4] C.B. Dover and J.M. Richard, Phys. Rev. C **21**, 1466 (1980).
[5] A. Faessler, G. Lübeck and K. Shimizu, Phys. Rev. D **26**, 3280 (1982).
[6] Hans-Peter Dürr, Phys. Rev. **109**, 1347 (1958).
[7] G. Goldhaber and J. Sandweiss, Phys. Rev. **110**, 1476 (1958).
[8] P. D. Barnes, S. Dytman, R. A. Eisenstein, W. C. Lam, J. Miller, R. B. Sutton, D. A. Jenkins and R. J. Powers, M. Eckhause, J. R. Kane, B. L. Roberts, R. E. Welsh, A. R. Kunselman, R. P. Redwine and R. E. Segel, Phys. Rev. Lett. **29**, 1132 (1972).
[9] G. Backenstoss, A. Bamberger, T. Bunaciu, J. Egger, H. Koch, U. Lynen, H. G. Ritter, H. A. Schmitt, A. Schwitter, Physics Letters B **41**, 552 (1972).
[10] P. Roberson, T. King, R. Kunselman, J. Miller, R.J. Powers, P.D. Barnes, R.A. Eisenstein, R.B. Sutton, C.R. Cox, M.Eckhause, J.R. Kane, A.M. Rushton, W.F. Vulcan, and R.E. Welsh, Phys. Rev C **16**, 1945 (1977).
[11] H. Poth, G. Backenstoss, I. Bergstrm, P. Blm, J. Egger, W. Fetscher, R. Guigas, R. Hagelberg, N. Hassler, C. J. Herrlander, M. Izycki, H. Koch, A. Nilsson, P. Pavlopoulos, H. P. Povel, K. Rolli, I. Sick, L. Simons, A. Schwitter, J. Sztarkier, and L. Tauscher, Nucl. Phys. A **294**, 435 (1978).
[12] E. Friedman and A. Gal, Phys. Rep. **452**, 89 (2007).
[13] E. H. Auerbach, C. B. Dover, and S. H. Kahana, Phys. Rev. Lett. **46**, 702 (1981).
[14] C.J. Batty, Nucl. Phys. A **372**, 433 (1981).
[15] R. Bonetti and M.S. Hussein, J. Phys. G: Nucl. Phys. **12**, L119 (1986).
[16] E. Friedman, A. Gal and J. Mares, Nucl. Phys. A **761**, 283 (2005).
[17] Stefan Teis, Wolfgang Cassing, Tomoyuki Maruyama and Ulrich Mosel, Phys. Rev. C **50**, 388 (1994).
[18] C. Spieles, M. Bleicher, A. Jahns, R. Mattiello, H. Sorge, H. Stöcker, and W. Greiner, Phys. Rev. C **53**, 2011 (1996).
[19] A. Sibirtsev, W. Cassing, G.I. Lykasov and M.V. Rzjanin, Nucl. Phys. A **632**, 131 (1998).
[20] I.N. Mishustin, L.M. Satarov, T.J. Bürvenich, H. Stöcker, and W. Greiner, Phys. Rev. C **71**, 035201 (2005).
[21] A.B. Larionov, I.N. Mishustin, L.M. Satarov, and W. Greiner, arXiv:0802.1845v2.
[22] P.D. Barnes, G. Diebold, G. Franklin, C. Maher, B. Quinn, J.Seydoux, K. Kilian, R. Besold, W. Eyrich, R. v. Frankenberg, A. Hofmann, D. Malz, F. Stinzing, P. Woldt, P. Birien, W. Dutty, J. Franz, H. Hamann, E. Rössle, H. Schledermann, H. Schmitt, H.-J. Urban, R.A. Eisenstein, D. Hertzog, W. Oelert, G. Sehl, B.E. Bonner, G. Ericsson, T. Johansson, S. Ohlsson, W.H. Breunlich, and P. Pawlek, Nucl. Phys. A **526**, 575 (1991).
[23] S. Pomp, *Hyperon Polarisation in the Reaction* $\overline{p}^{12}C \to \Lambda\overline{\Lambda}X$, Ph. D. thesis, Uppsala University (1999).
[24] I. Augustin, H.H. Gutbrod, D. Krämer, K. Langanke, H. Stöcker, Fourth International Conference on Fission and Properties of Neutron-Rich nuclei,Sanibel Island, Florida, 2007; arXiv:0804.0177v1 [hep-ph].
[25] $\overline{\text{P}}$ANDA Collaboration, Technical Progress Report (GSI Darmstadt), pp. 1-383 (2005).
[26] B. Hahn, D.G. Ravenhall, and R. Hofstadter, Phys. Rev. **101**, 1131 (1956).
[27] Review of Particle Physics, Particle Data Group, J. Phys. G: Nucl. Part. Phys. **33**, 1 (2006).
[28] A. Sibirtsev, K. Tsushima, and A.W. Thomas, Eur. Phys.J. A**6**, 351 (1999).
[29] H. Lenske and P. Kienle, Phys. Lett. B **647**, 82 (2007).
[30] E.J. Moniz, I. Sick, R.R. Whitney, J.R. Ficenec, R.D. Kephart, and W.P. Trower, Phys. Rev. Lett. **26**, 445 (1971).
[31] J.E. Wise, M.R. Braunstein, S. Hibrten, M.D. Kohler, B. J. Kriss, J. Ouyang, R.J. Peterson, J. A. McGill, C.L. Morris, S.J. Seestrom, R.M. Whitton, J.D. Zumbro, C.M. Edwards and A.L. Williams, Phys. Rev. C **48**, 1840 (1993).
[32] C.M. Kormanyos, R.J. Peterson, J.R. Shepard, J.E. Wise, S. Bart, R.E. Chrien, L. Lee, B.L. Clausen, J. Piekarewicz, M. B. Barakat, E.V. Hungerford, R.A. Michael, K.H. Hicks, and T. Kishimoto, Phys. Rev. C **51**, 669 (1995).
[33] Y. Fujii, O. Hashimoto, T. Nakagawa, Y. Sato, T. Takahashi, J. T. Brack, C. J. Gelderloos, M. V. Keilman, R. J. Peterson, M. Itoh, H. Sakaguchi, H. Takeda, K. Aoki, H. Hotchi, H. Noumi, Y. Ohta, H. Outa, M. Sekimoto, M. Youn, S. Ajimura, T. Kishimoto, H. Bhang, H. Park, and R. Sawafta, Phys. Rev. C **64**, 034608-1 (2001).
[34] F. Tabakin, R.A. Eisenstein, Y.Lu, Phys. Rev. C **44**, 1749 (1991).
[35] P.D. Barnes, G. Franklin, B. Quinn, R. Schumacher, V. Zeps, N. Hamann, W. Dutty, H. Fischer, J. Franz, E. Rössle, H. Schmitt, R. Todenhagen, R. v. Frankenberg, K. Kilian, W. Oelert, K. Röhrich, K. Sachs, T. Sefzick, M. Ziolkowski, R.A. Eisenstein, P.G. Harris, D.W. Hertzog, S.A. Hughes, P.E. Reimer, R.L. Tayloe, W. Eyrich, R. Geyer, M. Kirsch, R.A. Kraft, F. Stinzing, T. Johansson and S. Ohlsson, Phys. Rev. C **54**, 2831 (1996).
[36] H. Weber, E.L. Bratkovskaya, and H. Stöcker, Phys. Rev. C **66**, 054903 (2002).
[37] T. Yamazaki and Y. Akaishi, Phys. Lett. B **453**, 1 (1999).
[38] K. Tsushima and F.C. Khanna, Phys. Lett. B **552**, 138 (2003).
[39] K. Saito, K. Tsushima, and A.W. Thomas, Prog.Part.Nucl.Phys. **58**, 1 (2007).
[40] A.B. Kaidalov and P.E. Volkovitsky, Z. Phys. C **63**, 517 (1994).
[41] S. Grape, Licenciate thesis, Uppsala University (2008), arXiv:0805.0950v1; Physics Performance Report for $\overline{\text{P}}$ANDA (in preparation).
[42] W. Cassing, E.L. Bratkovskaya, and O. Hansen, Nucl. Phys. A **707**, 224 (2002).